Structural analysis of the N -acetyltransferase Eis1 from Mycobacterium abscessus reveals the molecular determinants of its incapacity to modify aminoglycosides

Kien Lam Ung, Laurent Kremer, Mickael Blaise

Structural analysis of the *N*-acetyltransferase Eis1 from *Mycobacterium abscessus* reveals the molecular determinants of its incapacity to modify aminoglycosides.

Running title: Crystal structure of *M. abscessus* Eis1

Kien Lam Ung[1], Laurent Kremer[1,2] and Mickaël Blaise*[1]

[1]Institut de Recherche en Infectiologie de Montpellier (IRIM), Université de Montpellier, CNRS UMR 9004, Montpellier, France.
[2]INSERM, IRIM, 34293 Montpellier, France.

*Corresponding author:
Tel: (+33)434359447; E-mail: mickael.blaise@irim.cnrs.fr

Abstract

Enhanced intracellular survival (Eis) proteins belonging to the superfamily of the GCN5-related *N*-acetyltransferases play important functions in mycobacterial pathogenesis. In *Mycobacterium tuberculosis,* Eis enhances the intracellular survival of the bacilli in macrophages by modulating the host immune response and is capable to chemically modify and inactivate aminoglycosides. In non-tuberculous mycobacteria (NTM), Eis shares similar functions. However, *Mycobacterium abscessus,* a multi-drug resistant NTM, possesses two functionally distinct Eis homologues, $Eis1_{Mab}$ and $Eis2_{Mab}$. While $Eis2_{Mab}$ participates in virulence and aminoglycosides resistance, this is not the case for $Eis1_{Mab,}$ whose exact biological function remains to be determined. Herein, we show that overexpression of $Eis1_{Mab}$ in *M. abscessus* fails to induce resistance to aminoglycosides. To clarify why $Eis1_{Mab}$ is unable to modify this class of antibiotics, we solved its crystal structure bound to its cofactor, acetyl-CoA. The structure revealed that $Eis1_{Mab}$ has a typical homohexameric Eis-like organization. The structural analysis supported by biochemical approaches demonstrated that while $Eis1_{Mab}$ can acetylate small substrates, its active site is too narrow to accommodate aminoglycosides. Comparison with other Eis structures showed that an extended loop between strands 9 and 10 is blocking the access of large substrates to the active site and movement of helices 4 and 5 reduces the volume of the substrate-binding pocket to these compounds in $Eis1_{Mab}$. Overall, this study underscores the molecular determinants explaining functional differences between $Eis1_{Mab}$ and $Eis2_{Mab,}$ especially those inherent to their capacity to modify aminoglycosides.

Keywords: *Mycobacterium abscessus*, *N*-acetyltransferase, aminoglycosides, Eis, GCN5, X-ray structure

Introduction

N-acetyltransferases are enzymes catalyzing the transfer of acyl groups from acyl-CoA to a wide panel of substrates, ranging from small molecules like spermine to large macromolecules, such as histones. Prokaryotic *N*-acetyltransferases belonging to the GCN5-related *N*-acetyltransferases family (GNAT) are capable to modify a large set of small substrates, including aminoglycoside antibiotics. They can exert pleiotropic effects, participating for instance in the biosynthesis of mycothiol, a mycobacterial antioxidant, or can modify bacterial peptides/proteins as well as host proteins in the case of pathogenic bacteria [1].

The Eis protein was initially discovered to confer enhanced survival of *Mycobacterium smegmatis* in macrophages, hence its designation as Enhanced Intracellular Survival [2]. Numerous studies have subsequently addressed the function of Eis from *Mycobacterium tuberculosis* (Eis_{Mtb}) emphasizing its capacity to modulate the host inflammatory response and autophagy [3,4,5] as well as its activity to acetylate various proteins, including the host histone H3 [3] and the mycobacterial nucleoid-associated protein HU [6].

In *M. tuberculosis* clinical strains, mutations in the *eis* promoter resulted in the up-regulation of *eis* expression and resistance to kanamycin [7]. The role of Eis_{Mtb} in the modification of aminoglycosides has been the subject of deep biochemical and structural investigations, demonstrating that its belongs to the GNAT superfamily of proteins. Eis_{Mtb} forms a homohexamer and can modify a wide range of aminoglycosides through mono- or poly-acetylations of their primary amine groups [8,9].

Consistent with these findings, the Eis2 protein ($Eis2_{Mab}$) has been shown to also play a key role in *Mycobacterium abscessus,* a non-tuberculous mycobacterium (NTM), recognized as an emerging human pathogen [10]. The *M. abscessus complex* comprises three subspecies, *M. abscessus sensu stricto*, *M. abscessus subsp. bolletii* and *M. abscessus subsp. massiliense* and has been associated with various clinical manifestations, including cutaneous, soft tissues, disseminated infections or lung infections. The pulmonary infections are particularly problematic to treat in the context of cystic fibrosis patients that are highly vulnerable to *M. abscessus complex* [11,12]. *M. abscessus* is also recognized as one of the most antibiotic-resistant mycobacterial species, leaving clinicians with few therapeutic options [13]. Standard drug regimens against *M. abscessus* lung diseases usually combine three antibiotic classes: an aminoglycoside (amikacin), a macrolide

(clarithromycin) and a *β*-lactam (cefoxitin or imipenem) [14]. However, *M. abscessus* is often refractory to these chemotherapies. The extreme resistance levels of this bacteria to most conventional antibiotics is notably well exemplified by the fact that *M. abscessus* is resistant to all first-line anti-tubercular drugs (isoniazid, rifampicin, pyrazinamide) [13].

In addition to drug target modification, resistance mechanisms in *M. abscessus* involve also intrinsic drug resistance, low permeability of the cell wall, induction of drug efflux pumps, absence or non-functional drug-activating enzymes which no longer convert pro-drugs into active metabolites.

Amikacin (AMK), a widely used antibiotic for the treatment of *M. abscessus* lung infection, is inactivated by the *N*-acetyltransferase $Eis2_{Mab}$ [17,18]. Biochemical and structural studies indicated that $Eis2_{Mab}$ accommodates a wide range of aminoglycosides in its active site where they are modified by the addition of one or several acetyl groups on their primary amine function, thus impeding their interaction with the ribosome [18,8]. Solving the high-resolution structure of $Eis2_{Mab}$ proved that this protein accommodates amikacin in its active site where the drug undergoes acetylation as supported in enzymatic assays [18]. Importantly, the deletion of $eis2_{Mab}$ increases the susceptibility of *M. abscessus* to aminoglycosides, thus supporting our findings [17]. Noteworthy, a recent study demonstrated the $Eis2_{Mab}$-dependent enhanced intracellular survival of *M. abscessus* in human macrophages, suggesting that $Eis2_{Mab}$ and Eis_{Mtb} share a similar biological function [19]. In contrast to *M. tuberculosis*, the *M. abscessus* genome encodes a second Eis protein homologous to $Eis2_{Mab}$, designated $Eis1_{Mab}$ and encoded by *MAB_4124*. However, inactivation of $eis1_{Mab}$ only modestly impacted the capacity of the mutant strain to infect macrophages and failed to modify the susceptibility to aminoglycosides as compared to an $eis2_{Mab}$ mutant [19]. This suggests that $Eis1_{Mab}$ and $Eis2_{Mab}$ share very limited overlapping functions [17,19]. The reasons for these differential biological functions between $Eis1_{Mab}$ and $Eis2_{Mab}$ remain obscure when considering the primary sequence identity (31%) between the two proteins. To fill this gap, and in order to provide the mechanistic basis explaining these differential aminoglycoside-modifying properties, a thorough structural and biochemical study of $Eis1_{Mab}$ was undertaken.

Materials and Methods

1- Inactivation of *eis1* in *M. abscessus*.

Deletion of *MAB_4124* ($eis1_{Mab}$) and *MAB_4532c* ($eis2_{Mab}$) in the reference strain *M. abscessus* CIP104536 was carried out using the double homologous recombination unmarked

strategy, reported previously [20]. The DNA sequences located upstream and downstream the *eis1*$_{Mab}$ gene were PCR-amplified and subsequently cloned into the pUX1-*katG* using the following primers and containing specific restriction sites (capital letters): fw_up_eis1_NheI 5'-gatcCGCTAGcccgaacccgtcgatacaggagttctcgtc-3'; rv_up__eis1_MfeI 5'-ggatcCAATTGcggtcacggcttcttgccctgtgttgtttc-3'; fw_down_eis1_MfeI 5'-gatccCAATTGacttctaggagtctgccgtgtcatccaggaac-3'; rv_down_eis1_HpaI 5'-ggatcGTTAACcaaggctagatgctcgcgcagcgtcgacccg-3'. The DNA sequences located upstream and downstream the *eis2* gene were PCR-amplified and subsequently cloned into the pUX1-*katG* plasmid using the following primers and containing specific restriction sites (capital letters): fw_up_eis2_HpaI: 5'-catccGTTAACctggagctgctccgatgagccgaaatatgc-3'; rv_up_eis2_MfeI: 5'-gatccCAATTGgtgcgtagggtcagctcagacacatacccatg-3'; fw_down_eis2_NheI: 5'-gatccGCTAGCgggatcgatcagcattactgtgtacagtcc-3'; rv_down_eis2_MfeI: 5'-gatccCAATTGgtttggctggcccgtcgcacccagtgcgcc-3'.

The resulting plasmids were introduced by electroporation in the smooth (S) variant of *M. abscessus* and the red fluorescent, kanamycin (KAN)-resistant colonies which underwent the first homologous recombination event were selected on Middlebrook 7H10 agar supplemented with 10% Oleic acid-Albumin-Dextrose-Catalase (OADC) in the presence of 200 μg.mL^{-1} KAN. Cultures of selected colonies were then subjected to a counter-selection on 7H10 agar plates supplemented with OADC containing 50 μg.mL^{-1} isoniazid (INH) to promote a second homologous recombination and removal of the KAN cassette. Non-fluorescent, INH-resistant colonies were picked up and further genotyped for *eis1*$_{Mab}$ deletion following PCR using two pairs of primers: fw_up_eis1_NheI with SQ2_b_down: 5'-cttactagaggagccatgggttctc-3' and SQ2_a_down: 5'-cgccaactccgttggtttggatatc-3' with SQ2_b_down. Identification of *eis2* mutants was performed by PCR using this pair of primers: SQ1_a_up: 5'-gctgggatgacggcggatgggacgg-3' and SQ1_b_up: 5'-ggtggagcgaatagatcgcgtcatg-3'. The positive clones were further confirmed by DNA sequencing of the genomic region surrounding the site of gene deletion.

For functional complementation of the *eis1*$_{Mab}$ deletion mutant (Δ*eis1*$_{Mab}$), the genomic sequence of *eis1*$_{Mab}$ was fused at its 5' end in frame with the sequence encoding the Streptag-II (italic letters), using the following primers (restriction sites in capital letters): fw_Eis1_261_NdeI 5'- ctcaaCATATGatg*TGGAGCCACCCGCAGTTCGAGAAG*atggccttcaccgcgcagcctcaatggcc-3' and rv_Eis1_261_HindIII 5'-caatgAAGCTTtcagaagttggtacctgcgaaaggttgc-3' and subsequently cloned into pMV261-Zeo [21] in which the kanamycin cassette has been replaced by a zeocine resistance cassette, between NdeI and HindIII. We used similar strategy to complement the Δ*eis2*$_{Mab}$ mutant by cloning the *eis2* gene into pMV261-Zeo using the following primers (restriction sites in capital

letters): fw_Eis2_261_NdeI 5'-ctcaaCATATGatg*TGGAGCCACCCGCAGTTCGAGAAG*atgtctgagctgaccctacgcaccattg -3' and rv_Eis2_261_HindIII 5'-caatgAAGCTTtcagaagtcgtcgggcgcactgggtgc-3'.

The parental, Δ*eis1 and Δeis2 M. abscessus* strains were transformed with either pMV261-Zeo, pMV261-Zeo-*eis1* or pMV261-Zeo-*eis2* and selected onto 7H10 agar supplemented with OADC and 50 μg.mL^{-1} Zeocin.

2-Amikacin susceptibility assessment.

The different strains were grown in Sauton's broth medium supplemented with 10%(v/v) OADC/ 0.025%(v/v) tyloxapol and 50 μg.mL^{-1} zeocin. The exponential bacterial cultures were pelleted and resuspended in PBS buffer. Five microliters of 10-fold serially diluted *M. abscessus* cultures were spotted on LB plates in the absence or presence of 4, 8 and 12 μg.mL^{-1} AMK. Plates were incubated at 37°C for 3 days.

3-Cloning, protein expression, and purification

The codon-optimized sequence (GenScript) encoding *eis1*$_{Mab}$ was cloned into pET-41 between the KpnI and EcoRI restriction sites in frame with the N-terminal Glutathione S-transferase (GST) tag followed by a Tobacco Etch Virus (TEV) protease cleavage site. An overnight culture of *Escherichia coli* BL21 (DE3) strain resistant to Phage T1 (New England Biolabs, Evry, France) carrying pRARE2 and transformed with pET41-*eis1*$_{Mab}$ was grown under agitation at 180 rpm at 37 ^{o}C in LB medium supplemented with 50 μg.mL^{-1} KAN and 30 μg.mL^{-1} chloramphenicol. This preculture was used to inoculate 6 L of LB broth supplemented with the same antibiotics at 37 ^{o}C. The cultures were cooled down in ice for 30 min when OD_{600} reached ~0.8 and protein expression was induced with 1 mM of Isopropyl-β-D-thiogalactoside (IPTG) (Euromedex) for 16 h at 18 °C. Cell pellets were collected by centrifugation at 6, 000 *g* for 20 min and resuspended in buffer A (50 mM Tris-HCl pH 8, 0.4 M NaCl, 1 mM β-mercaptoethanol, and 1 mM benzamidine). Bacteria were lysed by sonication and cell lysates were clarified by centrifugation at 28, 000 *g* at 4^{o}C for 1 h. The supernatant was then incubated 30 min with GST-sepharose beads with gentle agitation before being loaded onto a gravity column. Beads were washed with 10 column volumes of buffer B (50 mM Tris-HCl pH 8, 0.4 M NaCl, 1 mM β-mercaptoethanol) and buffer C (50 mM Tris-HCl pH 8, 1 M NaCl, 1 mM β-mercaptoethanol). Proteins were finally eluted with buffer D (50 mM Tris-HCl pH 8, 0.2 M NaCl, 1 mM β-mercaptoethanol and 15 mM glutathione). The eluate was incubated with TEV protease (1 mg of TEV protease per 40 mg of protein) and dialyzed overnight against

buffer E (20 mM Tris-HCl pH 8, 0.2 M NaCl, 1 mM β-mercaptoethanol). A Nickel-Nitrilotriacetic acid sepharose column was used to adsorb the His-tagged TEV protease, the cleaved tag and the uncleaved tagged protein. The tag-free protein that weakly binds to the column was collected by washing the column with buffer E supplemented with 50 mM imidazole. The protein was concentrated using a 10 kDa cut-off centricon (Sartorius) and purified by size-exclusion chromatography on a Superdex 200 Increase 10/300 GL column (GE Healthcare) with buffer F (20 mM Tris-HCl pH 8, 0.2 M NaCl). The protein concentration was determined using a Nanodrop 2000c spectrophotometer (Thermo Fisher Scientific) and the protein purity was estimated by Coomassie blue staining. $Eis2_{Mab}$ was expressed and purified, as described previously [18].

4-Enzyme kinetic assays

$Eis1_{Mab}$ and $Eis2_{Mab}$ were freshly purified in buffer F. The CoA-SH product of the acetyltransferase reaction triggers the reduction of DTNB (5,5-dithio-bis(nitrobenzoic acid) to form TNB (2-thio-5-nitrobenzoic acid, extinction coefficient: 14150 $M^{-1}.cm^{-1}$) with a peak of absorption at 412 nm. A master stock of KAN (containing 96% Kanamycin A and 4% KAN B), APR (Apramycin), ZEO (Zeocin), AMK (Amikacin), HYG (Hygromycin B), TYR (Tyramine), HIS (Histamine), acetyl-CoA (ACO) and enzymes were dissolved and diluted in buffer F. The premix A (enzyme, ACO, DTNB) and premix B (DTNB, substrate) were first incubated for 5 min at 25 ^{o}C. The reaction was initiated and measured immediately after combining both premixes to a final volume of 100 µL containing 0.25 µM enzyme, 0.5 mM ACO, 2 mM DTNB, and 5 mM of each substrate for assessment of the enzyme specificity. For kinetic constants determination one of the concentration either 5 mM TYR or 0.5 mM ACO was kept constant and the concentration of the other one varied. The reaction was followed at 25 ^{o}C and data points were recorded every 5 s for 90 s in a quartz cuvette and using a Nanodrop 2000c spectrophotometer (Thermo Fisher Scientific). All absorbance values were normalized against a negative control where the substrate was absent and standard errors were calculated from three replicates. Nonlinear least-squares regression was used to determine the Michaelis-Menten equation (Prism software, GraphPad).

5-Assessment of protein expression by Western-Blot

Single colonies were inoculated in 100 mL of Sauton's broth supplemented with 10%(v/v) OADC/0.025%(v/v) tyloxapol and 50 µg.mL^{-1} zeocin and grown for 3 days at 37 ^{o}C, under agitation at 120 rpm. Bacteria were harvested by centrifugation and resuspended in buffer A, described above. After opening bacteria by bead-beating and sonication, samples were centrifuged at 20, 000

g, at 4 °C. The supernatant was collected, mixed with loading-blue buffer and separated on SDS-PAGE. Proteins were then transferred onto a nitrocellulose membrane (GE Healthcare) in transfer buffer (20 mM Tris, 150 mM Glycine, 20% (v/v) ethanol). The membrane was saturated by blocking buffer (PBS 1X, 5% (m/v) skimmed milk, 0.2% (v/v) Tween 20) followed by incubation with primary monoclonal Anti-Strep-tag antibodies produced in mouse (dilution 1/10000) (Sigma-Aldrich). Bands were revealed by polyclonal anti-mouse antibodies conjugated to the horseradish peroxidase (dilution 1/5000) (Sigma-Aldrich). Protein were detected by the luminol-based reaction (SuperSignal™–Thermo Fisher Scientific) and imaged by a Chemidoc (Biorad).

6-Crystallization and x-ray data collection

Crystals were grown in sitting drops in MR Crystallization Plates™ (Hampton Research) at 18 °C by mixing 2 µL of protein solution concentrated to 0.4 $mg.mL^{-1}$ and containing 2 mM ACO with 2 µL of reservoir solution consisting of 0.8 M ammonium sulfate, 0.1 M Bis-Tris pH 5.5 and 1% (w/v) PEG 3350. Crystals were grown for one month and cryoprotected by a brief soaking step into a solution made of 1.4 M ammonium sulfate, 0.1 M Bis-Tris pH 5.5, 1% (w/v) PEG 3350 and 10% glycerol (v/v) prior being cryo-cooled in liquid nitrogen. X-ray diffraction data were collected at the Swiss-light source on the X06DA-PXIII beamline.

7-Structure solving and refinement

The $Eis1_{Mab}$ structure was solved by molecular replacement using the crystal structure of the $Eis2_{Mab}$ monomer bound to ACO (PDB: 6RFT) as a search request and sharing 31 % primary sequence identity with $Eis1_{Mab}$. *Molrep* from the CCP4i package [22] was used to performed molecular replacement. Six molecules were found in the asymmetric unit. After a first refinement step leading to R/Rfree of 0.46/0.5, *Autobuild* from the *Phenix* software suite [23] was further used to automatically improved the model building which led to R/Rfree: 0.32/0.41. The model was further manually rebuilt and refined using *Coot* [24] and the *Phenix* software suite. This led to a final model with refinement statistics shown in **Table 1**. The coordinates and structures factors have been deposited at the protein data bank under accession number: 6YCA.

Results

1-Overexpression of $Eis1_{Mab}$ does not induce aminoglycoside resistance in *M. abscessus*

A previous study reported that the deletion of e*is1*$_{Mab}$, but not *eis2*$_{Mab}$, was associated with an unchanged susceptibility profile to aminoglycosides, leading the authors to conclude that only *eis2*$_{Mab}$ participates in resistance to this class of antibiotics [17]. However, as emphasized by these authors, additional studies are required to confirm or dismiss the implication of Eis1$_{Mab}$ in aminoglycoside resistance, particularly by determining the antibiotic susceptibility pattern of a strain overexpressing Eis1$_{Mab}$. To address these two possibilities, *eis1*$_{Mab}$ was cloned into the episomal pMV261-Zeo construct under the control of the strong *hsp60* promoter, yielding pMV261-Zeo-*eis1,* to achieve high levels of protein expression. To easily monitor the expression of Eis1$_{Mab}$ by Western blotting, the protein was expressed as a fusion protein harboring a Streptag-II in its N-terminus. Moreover, a Δ*eis1*$_{Mab}$ deletion mutant was generated in the smooth variant of *M. abscessus* using a recently established recombineering procedure that allows the generation of unmarked gene deletion (Figure 1A and Figure 1B) [20]. Both the parental and Δe*is1*$_{Mab}$ strains were transformed with either the empty pMV261-Zeo or pMV261-Zeo-*eis1*. Zeocin was chosen as a selection marker as it does not belong to the aminoglycoside class of antibiotics and thus, the ZEO resistance cassette is very unlikely to affect the aminoglycoside susceptibility profile of the different strains tested. To include a control strain with increased susceptibility to aminoglycosides, we also generated a Δ*eis2*$_{Mab}$ deletion mutant known to be susceptible to AMK [17] and complemented strain (Figure S1).

Probing bacterial lysates of three independent clones using anti-Strep tag antibodies testified that high expression levels of Eis1$_{Mab}$ and Eis2$_{Mab}$ were achieved in both the wild-type, Δe*is1*$_{Mab}$ and *Δeis2*$_{Mab}$ strains carrying pMV261-Zeo-*eis1* or *pMV261-Zeo-eis2* (Figure 1C and Figure S1). Next, we tested whether overexpression of Eis1$_{Mab}$ in both wild-type and Δe*is1*$_{Mab}$ strains was associated with increased resistance to aminoglycosides on agar plates supplemented with increasing concentrations of APR, HYG or AMK. No major growth defect was noticed between the different strains plated on either drug as shown for AMK (Figure 1D). Conversely, the Δ*eis2*$_{Mab}$ mutant was hypersensitive to AMK as compare to all the other strains (Figure 1D). Overexpression of Eis2$_{Mab}$ in the mutant rescued this effect and growth occurred even in the presence of 12 μg.mL^{-1} of AMK, the highest concentration tested (Figure 1D). These results corroborate previous findings suggesting that unlike Eis2$_{Mab}$, Eis1$_{Mab}$ is not a primary determinant of resistance to aminoglycosides [17].

2-Eis1$_{Mab}$ is an active *N*-acetyltransferase but does not modify aminoglycosides

We next investigated the biochemical properties of $Eis1_{Mab}$. It was previously reported that recombinant $Eis1_{Mab}$ tends to aggregate, rendering the purification procedure challenging [8]. Likewise, we were facing the same issues when $Eis1_{Mab}$ was fused to small tags at its N-terminus, such as His- and S-tags. This tendency to aggregate may suggest a folding issue of the protein and, may explain, at least partly, the lack of activity of $Eis1_{Mab}$ [8]. To circumvent this problem, we attempted to increase protein solubility by overexpressing $Eis1_{Mab}$ fused to the Glutathione-S-transferase (GST) in its N-terminus. This greatly increased the solubility of the protein and to purify it *via* a three-step purification procedure. $Eis1_{Mab}$ did not aggregate after removal of the GST-tag and, as long it was not too concentrated, a homogeneous and sharp peak could be observed on gel-filtration (Figure 2). The size-exclusion elution profile strongly suggests that $Eis1_{Mab}$ behaves as a multimer in solution. A calibration curve allowed to calculate an apparent molecular weight of 198 kDa, similar to the one reported for its closest homologue $Eis2_{Mab}$ [18] or to those of Eis from *M. tuberculosis* or *M. smegmatis* [25]. From this, it can be inferred that $Eis1_{Mab}$ is a hexamer in solution.

The substrate specificity of $Eis1_{Mab}$ was next assessed *in vitro* by enzymatic assay but no activity was detected towards a range of aminoglycoside antibiotics. However, an *N*-acetyltransferase activity was detected when using arylalkylamine substrates, such as TYR and HIS (Figure 3A and 3B). These two substrates are smaller compare with aminoglycosides (Figure 3A) and possess primary amine groups. TYR and HIS are known to be acetylated by different *N*-acetyltransferases and are substrates of Eis from *M. tuberculosis* and *M. smegmatis* [26]. Interestingly, $Eis1_{Mab}$ was found to be more active towards TYR and HIS than $Eis2_{Mab}$ (Figure 3B).

This prompted us to determine the kinetic constants of $Eis1_{Mab}$ for TYR, which appears as the preferred substrate of the enzyme (Figure 3B). As could be expected for noncognate substrates the K_M= 722 ± 21 μM and k_{cat}= 11 ± 0.5 s^{-1} for TYR are suggestive of moderate activity. $Eis1_{Mab}$ displays also a slightly lower affinity ($K_{M=}$ 144 ± 19 μM) for ACO as compared to $Eis2_{Mab}$ (K_M= 36.2 ± 2.9 μM) [18] and to Eis homologous proteins [8] which all display K_M values < 50 μM (Figure 3C). Nonetheless, these *in vitro* data support the view that $Eis1_{Mab}$ purified under our experimental procedure is an active *N*-acetyltransferase and, in contrast to $Eis2_{Mab,}$ does not modify aminoglycosides. The smaller substrate preference of $Eis1_{Mab}$ as compared to $Eis2_{Mab}$ makes it a noticeable feature that distinguishes the two enzymes.

3-Overall crystal structure of $Eis1_{Mab}$

To get insights into the molecular basis driving the $Eis1_{Mab}$ substrate specificity, we aimed at resolving the crystal structure of the protein. Extensive screening for crystallization conditions

using either the *apo*- or ACO-bound form of $Eis1_{Mab}$ generated numerous crystals. However, only crystals of the (ACO)-bound form of $Eis1_{Mab}$ allowed the collection of exploitable datasets. We solved the crystal structure by molecular replacement using $Eis2_{Mab}$ as a search model and the model was refined to a resolution of 2.9 Å (Table 1). Most residues could be modeled except for the first 23 N-terminus amino acids and part of helix 2 in all monomers.

The overall structure of $Eis1_{Mab}$ is a multimer formed by six monomers. This hexameric architecture is similar to the organization of proteins belonging to the GNAT superfamily and also to $Eis2_{Mab}$ and to its homologues in *M. tuberculosis* (Eis_{Mtb}) and *M. smegmatis* (Eis_{Msm}). It consists of the superposition of two homotrimers with a central vestibule (Figure 4A). This oligomeric state fully agrees with the apparent molecular mass determined by size-exclusion chromatography (Figure 2). The structure of the $Eis1_{Mab}$ monomer can be divided into three subdomains: the N-terminal GNAT domain (residues 1-135), the central GNAT domain (residues 136-312) and the C-terminal domain (residues 313-415). Each monomer is composed of seventeen β-strands (β1 to β17), ten α-helices (α1 to α10) and seven 3_{10} helices (η1 to η7) (Figure 4B).

4-The Acetyl-CoA binding site of $Eis1_{Mab}$

The best diffracting $Eis1_{Mab}$ crystals were obtained in the presence of ACO. The simulated-annealed OMIT electron density map certifies the presence of the cofactor in the $Eis1_{Mab}$ structure (Figure 4C). Due to the medium resolution, no water molecule could be modeled but fourteen residues involved in cofactor recognition could be identified (Figure 4D). While the side chains of Leu135 and Ile142 are involved in hydrophobic interactions, the His101 main chain provides a weak H-bond with the oxygen of the acetyl moiety. The carbonyl of Ile102 and Val104 establish also H-bonds. The ACO phosphate groups are recognized by the main chains of Arg110, Gly112, Ile114, and Thr115, as well as by the side chain of Thr115. Arg110 plays a key role in the interaction by making a salt-bridge with the phosphate group, creating a H-bond with the O group and a stacking interaction with the adenine ring of ACO. The carboxyl group of Glu139 binds to the NH2 of the adenine ring whereas Ser138 interacts with the O group of ACO. The Arg145 guanidium group recognizes the O4 of the ribose of ACO (Figure 4D). Additionally, multiple primary sequence alignments indicate that the cofactor binding site is relatively well conserved among the mycobacterial Eis proteins (Figure 5). Therefore, we rule out the possibility that these few amino acid substitutions in the cofactor binding site of $Eis1_{Mab}$ would explain the difference of the substrate specificity between $Eis1_{Mab}$ and the other Eis proteins.

5- The structural basis for Eis1$_{Mab}$ substrate specificity

We next searched at the Protein Data Dank using the eFOLD (https://www.ebi.ac.uk/msd-srv/ssm/) and DALI [27] servers for the closest homologues of Eis1$_{Mab}$. First of all, we superposed Eis homologues structures from proteins that have been biochemically characterized and have been reported to modify aminoglycosides [8,28,29]. The multiple sequence alignments (Figure 5) and superposition of the Eis1$_{Mab}$ monomer to the other Eis:ACO or Eis:CoA bound structures (Figure 6A) generated the following primary sequence identity and root mean square deviation (r.m.s.d.) values: Eis$_{Mtb}$ (PDB id: 3RYO, 30% identity, r.m.s.d. 1.8 Å) [30], Eis$_{Msm}$ (PDB id: 3SXN, 31% identity and r.s.m.d. 1.8 Å) [30], Eis2$_{Mab}$ (PDB id: 6RFT, 31% seq identity, r.m.s.d. 2.1 Å) [18] and *Anabaena variabilis*, Eis$_{Ava}$, (PDB id: 2OZG, 20% and r.m.s.d. 2.2 Å), unpublished. Additionally, the structure of Eis$_{Ban}$ from *Bacillus anthracis* (PDB id: 3N7Z) [29] solved without cofactor displays low sequence identity, 17% but a similar r.s.m.d of 2.1 Å. Our search allowed the comparison of two other Eis homologues that were not biochemically characterized, for instance, the Eis$_{Efa}$ from *Enterococcus faecalis,* with no ligand (PDB id: 2I00, 17%, r.m.s.d. 2.10 Å), and Eis$_{Kfl}$ from *Kribbella flavida* (PDB id: 4MY0, 21%, r.m.s.d. 2.4 Å). This structural comparison indicate that the closest homologues of Eis1$_{Mab}$ are Eis proteins from the mycobacterium phylum.

To understand the structural features responsible for Eis1$_{Mab}$'s preferences for small substrates, the crystal structure of Eis1$_{Mab}$ was compared with those of Eis$_{Mtb}$ and Eis$_{Msm}$ which were solved in the presence of aminoglycosides. Eis$_{Mtb}$ was co-crystallized with tobramycin (PDB id: 4JD6) [9] and Eis$_{Msm}$ with paromomycin (PDB id: 4QB9) [31]. Most residues seen interacting with tobramycin in Eis1$_{Mab}$ are not conserved except for the ultra-conserved carboxy-terminal Phe residue (Figure 5). Furthermore, among the eleven residues contacting paromomycin in Eis$_{Msm}$, only three residues are semi-conserved (Thr100, His101, and Glu307) in Eis1$_{Mab}$ while two others are strictly conserved (Ser138 and Phe415 at the C-terminus) (Figure 5). However, due to the partial conservation in the overall primary sequence between Eis$_{Mtb}$, Eis$_{Msm}$, and Eis2$_{Mab}$ (Figure 5), it remains difficult to state that the inability of Eis1$_{Mab}$ to modify aminoglycosides is inherent to the absence of amino acids conservation in the substrate-binding pocket. We, therefore, hypothesized that the size of Eis1$_{Mab}$ active site pocket may be reduced as compared with other Eis proteins. Determination of the central cavity volume that includes both the cofactor and substrate binding sites of each Eis protein was carried out with the CASTp server and, using its default settings [32]. This analysis showed that Eis1$_{Mab}$ has a rather small cavity of 651 Å^3 in comparison with the other Eis members that were experimentally shown to acetylate aminoglycosides (2005 Å^3 for Eis$_{Mtb}$, 1678 Å^3 for Eis$_{Msm}$, 1371 Å^3 for Eis$_{Ava}$ and 1274 Å^3 for Eis2$_{Mab}$). Only Eis$_{Ban}$ has a slightly bigger volume than Eis1$_{Mab}$ (695 Å^3) (Figure 6B). Comparison of Eis1$_{Mab}$ with Eis$_{Mtb}$, which possesses the

largest cavity allows proposing that the small cavity in $Eis1_{Mab}$ results of the positioning of helix 4 which pushes further away helix 5. Consequently, this places the bulky side chains of residues Trp205, His210, and Phe213 closer to the Phe415 at the C-terminus, known to be required for substrate recognition (Figure 6C). These structural features reducing the volume of the $Eis1_{Mab}$ substrate cavity are not seen in Eis_{Mtb}, as the less bulky side chains of the equivalent residues Leu196, Leu200 and Glu202 are not protruding into the aminoglycoside-binding cavity (Figure 6C).

The structural comparison of the various Eis proteins unraveled an atypical feature in the central GNAT domain of $Eis1_{Mab}$ (Figure 5 and Figure 6A). The region composed of fourteen residues and ranging from residues 235 to 248 (235-PQDTAEWFSSSART-248) is forming a loop and a 3_{10} helix (η4, Figure 4B). This region spanning between strands β9 and β10 is extended in $Eis1_{Mab}$ as compared with the other Eis proteins. This loop seems to act as a lid covering the substrate-binding site of the neighbor subunit (Figure 7A). Hence, this region might restrict the accessibility of the substrate-binding pocket to bulky molecules. Furthermore, Phe242, which is not conserved in other Eis homologues (Figure 5) seems of particular interest since its bulky side chain is protruding into the substrate-binding pocket, as can be appreciated when $Eis1_{Mab}$ is superposed onto the tobramycin-bound Eis_{Mtb} structure (Figure 7A). This may further reduce the volume of the substrate-binding site, thus compromising the access to large substrates, like aminoglycosides. Of note, this loop between strands β9 and β10 as well as Phe242 is strictly conserved in all subspecies of the *M. abscessus complex* (data not shown). Moreover, the corresponding loop was found to be much shorter in all the Eis proteins for which the enzymatic activity towards aminoglycosides was experimentally demonstrated. The loop of Eis_{Mtb} or Eis_{Msm} possesses 8 residues (228-VDRTDLKL-235) and 7 residues (226-RGPDGRR-232), respectively (Figure 7B). Additionally, even shorter loops are seen in two other Eis proteins whose activity towards aminoglycosides was demonstrated [29,28] the loops in the Eis_{Ban} (219-ENYK-222) and Eis_{Ava} (221-RTRDGS-226) crystal structures are made of 4 and 6 residues, respectively (Figure 7B).

Discussion

Mycobacterial *N*-acetyltransferases and particularly Eis proteins play important roles in macrophage invasion, persistence, modulation of the immune response and antibiotic resistance [33]. *Eis* proteins modify a large set of aminoglycosides and have an impact on antibiotic resistance in numerous mycobacterial species, notably in *M. tuberculosis* and in NTM, including *M. abscessus* [18,17] and *M. fortuitum* [33]. Thus, molecules inhibiting Eis proteins given in combination with aminoglycosides would broaden the efficacy of this class of antibiotics in the fight against mycobacterial infections [34]. The other biological functions of Eis protein related to the enhanced

intracellular survival or to the modulation of the immune response of the host are also of interest in terms of druggability. Despite being closely related, the contribution of $Eis1_{Mab}$ and $Eis2_{Mab}$ to the intracellular survival of *M. abscessus* differs. While the deletion of *eis1*$_{Mab}$ only slightly impairs the survival of *M. abscessus* in macrophages, the deletion of *eis2*$_{Mab}$ profoundly affects the intracellular survival of the mutant strain [19]. Additionally, regulation of the intracellular expression of the two genes is opposite as *eis1*$_{Mab}$ is downregulated while *eis2*$_{Mab}$ is upregulated in *M. abscessus*-infected macrophages [19]. Importantly, our study unambiguously establishes that in contrast to $Eis2_{Mab}$, $Eis1_{Mab}$ is not implicated in resistance to aminoglycosides, supporting previous findings [8,17,35]. This absence of redundant function between the two Eis homologues makes $Eis2_{Mab}$ as an interesting drug target to explore further to tackle drug resistance and virulence of *M. abscessus*.

Solving the crystal structure of $Eis1_{Mab}$ sheds new light into the differential biological functions of Eis proteins in general and $Eis1_{Mab}$ and $Eis2_{Mab}$ more particularly. Structural comparison of many Eis structures belonging to the Mycobacterium or to other phyla identified key structural elements that are likely to block the access of $Eis1_{Mab}$ binding site to large substrates such as aminoglycosides. In particular, the existence of an extended loop acting as a lid and covering the active site of the neighbor monomer as well as the positioning of helices 4 and 5 restrict the accessibility to the active site. Future work should be dedicated to investigating in more detail the substrate specificity of $Eis1_{Mab}$ by creating defined mutants in the extended loop and/or α4-α5 helices. This appears achievable as modulation of the Eis_{Mtb}'s substrate specificity was successfully done by mutating bulky residues that restrict the entrance of the active site [36].

This work may also add meaningful information allowing to predict the Eis-like protein substrate specificity. Like *M. abscessus*, other mycobacterial species possess several paralogues of the Eis protein [33], and predicting the function of these proteins particularly in the case of pathogenic bacteria may help to anticipate whether these Eis-like proteins may play a role in resistance to aminoglycosides. In that regard, bioinformatics tools such as multiple primary sequence alignments combine with protein structure homology modeling, could be useful to estimate the size of the loop between strands 9 and 10 (or strands 10 and 11 depending of the Eis origin) of the Eis homologues and consequently their substrate specificity.

While $Eis1_{Mab}$ cannot modify aminoglycosides, our results indicate that it is an active *N*-acetyltransferase towards the small TYR and HIS arylalkylamine compounds, which are very unlikely the "natural substrates" of the enzyme. In the quest of identifying possible substrate of $Eis1_{Mab}$ we carefully analyzed the genomic environment around *eis1*$_{Mab}$, and found that it probably belongs to an operon that is extremely well conserved among all the three *M. abscessus* subspecies and in other NTM, such as *Mycobacterium chelonae*, *Mycobacterium saopaulense* or

Mycobacterium immunogenum. This operon also encompasses genes coding for a putative permease (*MAB_4122*), a predicted monooxygenase/acyl-CoA dehydrogenase (*MAB_4123*) located upstream of *eis1*$_{Mab}$ and a nitrilotriacetate monooxygenase (*MAB_4125*) possessing a bacterial luciferase predicted domain, downstream of *eis1*$_{Mab}$. *MAB_4122* and *MAB_4125* are close homologues of the dibenzothiophene desulfurization enzymes A and C present in numerous bacteria able to degrade dibenzothiophene, an organosulfur compound found in petroleum [37]. Interestingly, the existence of such degradation pathway has also been described in *Mycobacterium phlei* [38], which also possesses one Eis-like protein. Although Eis-like *N*-acetyltransferases have not been found yet functionally linked to such degradation pathway, this conserved genomic organization suggests that Eis1$_{Mab}$ might be a new partner of this organosulfur chemicals degradation/detoxification pathway. This may be relevant to the fact that NTMs are environmental bacteria, which are likely to encounter organosulfur compounds in their ecological niche. In addition, that dibenzothiophene derivatives are also potent inhibitors of *M. tuberculosis* [39] may suggest that the *eis1*$_{Mab}$ operon participates in resistance of *M. abscessus* to these compounds.

Conflict of interest statement

The authors declare no conflict of interest.

Acknowledgements

We thank the staff at SLS beamlines for support during data collection, the Fondation pour la Recherche Médicale (FRM) [grant number DEQ20150331719 to LK], and A. Viljoen for fruitful discussion. KLU Ph.D. fellowship is supported by the National Research Agency [ANR-17-CE11-0008-01 – MyTraM to MB]

Author contributions

KLU and MB designed and performed experiments. MB and LK supervised research. MB wrote the first draft with input of all the authors.

References

1. Favrot L, Blanchard JS, Vergnolle O (2016) Bacterial GCN5-Related N-Acetyltransferases: From Resistance to Regulation. Biochemistry 55:989–1002.

2. Wei J, Dahl JL, Moulder JW, Roberts EA, O'Gaora P, Young DB, Friedman RL (2000) Identification of a Mycobacterium tuberculosis gene that enhances mycobacterial survival in macrophages. J. Bacteriol. 182:377–384.

3. Duan L, Yi M, Chen J, Li S, Chen W (2016) Mycobacterium tuberculosis EIS gene inhibits macrophage autophagy through up-regulation of IL-10 by increasing the acetylation of histone H3. Biochem. Biophys. Res. Commun. 473:1229–1234.

4. Samuel LP, Song C-H, Wei J, Roberts EA, Dahl JL, Barry CE, Jo E-K, Friedman RL (2007) Expression, production and release of the Eis protein by Mycobacterium tuberculosis during infection of macrophages and its effect on cytokine secretion. Microbiol. Read. Engl. 153:529–540.

5. Shin D-M, Jeon B-Y, Lee H-M, Jin HS, Yuk J-M, Song C-H, Lee S-H, Lee Z-W, Cho S-N, Kim J-M, et al. (2010) Mycobacterium tuberculosis eis regulates autophagy, inflammation, and cell death through redox-dependent signaling. PLoS Pathog. 6:e1001230.

6. Ghosh S, Padmanabhan B, Anand C, Nagaraja V (2016) Lysine acetylation of the Mycobacterium tuberculosis HU protein modulates its DNA binding and genome organization. Mol. Microbiol. 100:577–588.

7. Zaunbrecher MA, Sikes RD, Metchock B, Shinnick TM, Posey JE (2009) Overexpression of the chromosomally encoded aminoglycoside acetyltransferase eis confers kanamycin resistance in Mycobacterium tuberculosis. Proc. Natl. Acad. Sci. U. S. A. 106:20004–20009.

8. Green KD, Pricer RE, Stewart MN, Garneau-Tsodikova S (2015) Comparative Study of Eis-like Enzymes from Pathogenic and Nonpathogenic Bacteria. ACS Infect. Dis. 1:272–283.

9. Houghton JL, Biswas T, Chen W, Tsodikov OV, Garneau-Tsodikova S (2013) Chemical and structural insights into the regioversatility of the aminoglycoside acetyltransferase Eis. Chembiochem Eur. J. Chem. Biol. 14:2127–2135.

10. Johansen MD, Herrmann J-L, Kremer L (2020) Non-tuberculous mycobacteria and the rise of Mycobacterium abscessus. Nat. Rev. Microbiol. 18:392–407.

11. Roux A-L, Catherinot E, Ripoll F, Soismier N, Macheras E, Ravilly S, Bellis G, Vibet M-A, Le Roux E, Lemonnier L, et al. (2009) Multicenter study of prevalence of nontuberculous mycobacteria in patients with cystic fibrosis in france. J Clin Microbiol 47:4124–4128.

12. Dedrick RM, Guerrero-Bustamante CA, Garlena RA, Russell DA, Ford K, Harris K, Gilmour KC, Soothill J, Jacobs-Sera D, Schooley RT, et al. (2019) Engineered bacteriophages for treatment of a patient with a disseminated drug-resistant Mycobacterium abscessus. Nat. Med. 25:730–733.

13. Nessar R, Cambau E, Reyrat JM, Murray A, Gicquel B (2012) Mycobacterium abscessus: a new antibiotic nightmare. J Antimicrob Chemother 67:810–818.

14. Strnad L, Winthrop KL (2018) Treatment of Mycobacterium abscessus Complex. Semin. Respir. Crit. Care Med. 39:362–376.

15. Richard M, Gutiérrez AV, Kremer L (2020) Dissecting erm(41)-Mediated Macrolide-Inducible Resistance in Mycobacterium abscessus. Antimicrob. Agents Chemother. 64:e01879-19.

16. Luthra S, Rominski A, Sander P (2018) The Role of Antibiotic-Target-Modifying and Antibiotic-Modifying Enzymes in Mycobacterium abscessus Drug Resistance. Front. Microbiol. 9:2179.

17. Rominski A, Selchow P, Becker K, Brülle JK, Dal Molin M, Sander P (2017) Elucidation of Mycobacterium abscessus aminoglycoside and capreomycin resistance by targeted deletion of three putative resistance genes. J. Antimicrob. Chemother. 72:2191–2200.

18. Ung KL, Alsarraf HMAB, Olieric V, Kremer L, Blaise M (2019) Crystal structure of the aminoglycosides N-acetyltransferase Eis2 from Mycobacterium abscessus. FEBS J. 286:4342–4355.

19. Dubois V, Pawlik A, Bories A, Le Moigne V, Sismeiro O, Legendre R, Varet H, Rodríguez-Ordóñez MDP, Gaillard J-L, Coppée J-Y, et al. (2019) Mycobacterium abscessus virulence traits unraveled by transcriptomic profiling in amoeba and macrophages. PLoS Pathog. 15:e1008069.

20. Richard M, Gutiérrez AV, Viljoen A, Rodriguez-Rincon D, Roquet-Baneres F, Blaise M, Everall I, Parkhill J, Floto RA, Kremer L (2019) Mutations in the MAB_2299c TetR Regulator Confer Cross-Resistance to Clofazimine and Bedaquiline in Mycobacterium abscessus. Antimicrob. Agents Chemother. 63:e01316-18.

21. Stover CK, de la Cruz VF, Fuerst TR, Burlein JE, Benson LA, Bennett LT, Bansal GP, Young JF, Lee MH, Hatfull GF (1991) New use of BCG for recombinant vaccines. Nature 351:456–460.

22. Winn MD, Ballard CC, Cowtan KD, Dodson EJ, Emsley P, Evans PR, Keegan RM, Krissinel EB, Leslie AGW, McCoy A, et al. (2011) Overview of the CCP4 suite and current developments. Acta Crystallogr. D Biol. Crystallogr. 67:235–242.

23. Adams PD, Afonine PV, Bunkóczi G, Chen VB, Davis IW, Echols N, Headd JJ, Hung L-W, Kapral GJ, Grosse-Kunstleve RW, et al. (2010) PHENIX: a comprehensive Python-based system for macromolecular structure solution. Acta Crystallogr. D Biol. Crystallogr. 66:213–221.

24. Emsley P, Lohkamp B, Scott WG, Cowtan K (2010) Features and development of Coot. Acta Crystallogr. D Biol. Crystallogr. 66:486–501.

25. Anand S, Ganaie AA, Sharma C (2019) Differential thermal stability, conformational stability and unfolding behavior of Eis proteins from Mycobacterium smegmatis and Mycobacterium tuberculosis. PLOS ONE 14:e0213933.

26. Pan Q, Zhao F-L, Ye B-C (2018) Eis, a novel family of arylalkylamine N-acetyltransferase (EC 2.3.1.87). Sci. Rep. 8:1–8.

27. Holm L, Rosenström P (2010) Dali server: conservation mapping in 3D. Nucl Acids Res 38:W545–W549.

28. Pricer RE, Houghton JL, Green KD, Mayhoub AS, Garneau-Tsodikova S (2012) Biochemical and structural analysis of aminoglycoside acetyltransferase Eis from Anabaena variabilis. Mol. Biosyst. 8:3305–3313.

29. Green KD, Biswas T, Chang C, Wu R, Chen W, Janes BK, Chalupska D, Gornicki P, Hanna PC, Tsodikov OV, et al. (2015) Biochemical and structural analysis of an Eis family aminoglycoside acetyltransferase from bacillus anthracis. Biochemistry 54:3197–3206.

30. Kim KH, An DR, Song J, Yoon JY, Kim HS, Yoon HJ, Im HN, Kim J, Kim DJ, Lee SJ, et al. (2012) Mycobacterium tuberculosis Eis protein initiates suppression of host immune responses by acetylation of DUSP16/MKP-7. Proc. Natl. Acad. Sci. U. S. A. 109:7729–7734.

31. Kim KH, An DR, Yoon HJ, Yang JK, Suh SW (2014) Structure of Mycobacterium smegmatis Eis in complex with paromomycin. Acta Crystallogr. Sect. F Struct. Biol. Commun. 70:1173–1179.

32. Tian W, Chen C, Lei X, Zhao J, Liang J (2018) CASTp 3.0: computed atlas of surface topography of proteins. Nucleic Acids Res. 46:W363–W367.

33. Sanz-García F, Anoz-Carbonell E, Pérez-Herrán E, Martín C, Lucía A, Rodrigues L, Aínsa JA (2019) Mycobacterial Aminoglycoside Acetyltransferases: A Little of Drug Resistance, and a Lot of Other Roles. Front. Microbiol. 10:46.

34. Ngo HX, Green KD, Gajadeera CS, Willby MJ, Holbrook SYL, Hou C, Garzan A, Mayhoub AS, Posey JE, Tsodikov OV, et al. (2018) Potent 1,2,4-Triazino[5,6 b]indole-3-thioether Inhibitors of the Kanamycin Resistance Enzyme Eis from Mycobacterium tuberculosis. ACS Infect. Dis. 4:1030–1040.

35. Hurst-Hess K, Rudra P, Ghosh P (2017) Mycobacterium abscessus WhiB7 Regulates a Species-Specific Repertoire of Genes To Confer Extreme Antibiotic Resistance. Antimicrob. Agents Chemother. 61:e01347-17.

36. Jennings BC, Labby KJ, Green KD, Garneau-Tsodikova S (2013) Redesign of substrate specificity and identification of the aminoglycoside binding residues of Eis from Mycobacterium tuberculosis. Biochemistry 52:5125–5132.

37. Bhanjadeo MM, Rath K, Gupta D, Pradhan N, Biswal SK, Mishra BK, Subudhi U (2018) Differential desulfurization of dibenzothiophene by newly identified MTCC strains: Influence of Operon Array. PLOS ONE 13:e0192536.

38. Kayser KJ, Cleveland L, Park H-S, Kwak J-H, Kolhatkar A, Kilbane JJ (2002) Isolation and characterization of a moderate thermophile, Mycobacterium phlei GTIS10, capable of dibenzothiophene desulfurization. Appl. Microbiol. Biotechnol. 59:737–746.

39. Surineni G, Marvadi SK, Yogeeswari P, Sriram D, Kantevari S (2018) Dibenzofuran, dibenzothiophene and N-methyl carbazole tethered 2-aminothiazoles and their cinnamamides as potent inhibitors of Mycobacterium tuberculosis. Bioorg. Med. Chem. Lett. 28:1610–1614.

40. Robert X, Gouet P (2014) Deciphering key features in protein structures with the new ENDscript server. Nucleic Acids Res. 42:W320–W324.

Figure legends

Figure 1: Aminoglycosides susceptibility assessment of Eis1-overexpressing *M. abscessus* strains.

A Schematic representation of the genomic region around *eis1* in the parental (WT) and Δ*eis1* mutant strains of *M. abscessus*. Sizes of the PCR amplicons used for genotyping of the Δ*eis1* mutant are shown. **B** PCR profile confirming the proper deletion of *eis1* in the mutant strain. Two PCR products of 1.8 and 2.9 kb were amplified from Δ*eis1* genomic DNA while two bands at 4 and 2.9 kb are expected for the WT strain. **C** Protein expression pattern of $Eis1_{Mab}$ in parental (WT) and knockout strains. Western blotting using anti-Strep-tag primary antibodies attest for the expression of $Eis1_{Mab}$ in the two strains transformed with pMV261-Zeo-*eis1* in three individual colonies (C1-C3). Strain transformed with the empty pMV261-Zeo were included as negative controls. The band at 70kDa of the protein ladder possesses also a Strep-tag explaining its immune reactivity with the antibody. **D** Amikacin susceptibility profile of parental (WT), Δ*eis1 M. abscessus* strains overexpressing $Eis1_{Mab}$ and Δ*eis2 M. abscessus* strains overexpressing $Eis2_{Mab}$. Serial dilutions of bacteria carrying either pMV261-Zeo, pMV261-Zeo-*eis1* or pMV261-Zeo-*eis2* were spotted onto LB agar supplemented with increasing concentrations of AMK and incubated at 37 °C for 3 days. The figure is representative of two independent experiments.

Figure 2: Determination of the oligomeric state of $Eis1_{Mab}$

Estimation of the oligomeric state of recombinant $Eis1_{Mab}$ by size-exclusion chromatography (left panel). The elution profile of the proteins used for calibration is displayed as a black line and the elution profile of $Eis1_{Mab}$ is shown in red. The calibration curve was established using *β*-amylase (1) (200 kDa), bovine serum albumin (2) (66 kDa), carbonic anhydrase (3) (29 kDa) and cytochrome C (4) (12.4 kDa), eluted with estimated volumes of 11.02, 13.2, 15.8 and 17.4 mL, respectively. The void volume corresponds to the dextran blue elution peak at 8.5 mL. The elution peak of $Eis1_{Mab}$ at 10.9 mL matches an apparent molecular weight of 198 kDa. Coomassie Blue-stained SDS polyacrylamide gel electrophoresis of $Eis1_{Mab}$ produced after the last step of purification on size-exclusion chromatography (10 µg of protein; right panel).

Figure 3: Biochemical characterization and enzymatic activity of $Eis1_{Mab}$.

A Chemical structures of the different substrates tested in the assay. The structure of zeocin which is a very large molecule is not displayed. **B** Initial rates of $Eis1_{Mab}$ determined in the presence of various substrates, including apramycin, hygromycin, kanamycin, zeocin, tyramine and histamine at a concentration of 5 mM. As a positive control, purified $Eis2_{Mab}$ was also tested with TYR and HIS. **C** Michaelis and Menten curves used to determine the kinetic constants for TYR (left panel) and ACO (right panel).

Figure 4: Overall three-dimensional structure of $Eis1_{Mab}$.

A Overall crystal structure of $Eis1_{Mab}$ bound to ACO. The structure of the $Eis1_{Mab}$ hexamer is depicted as a cartoon representation where each chain is colored differently. The left panel is a top view of the structure and the right one is rotated by 90°. ACO is pictured in each chain as a sphere representation. **B** Cross-eye stereo view of the $Eis1_{Mab}$ monomer**.** The three domains are displayed as a cartoon representation where the N-terminal (Nt) GNAT domain is displayed as raspberry color, the central GNAT domain is in blue and the C-terminal (Ct) GNAT domain is in yellow. α, β and η indicate α-helices, β-strands, and 3_{10} helices respectively. **C** Fo-Fc simulated-annealed OMIT map. The electron density map surrounding the ACO ligand is displayed as a grey mesh and contoured at 2.8 σ level. **D** ACO interactions with the Eis1 residues are shown as white sticks. Hydrogen-bond and the salt-bridge interactions are shown as black dashed lines.

Figure 5: Structural comparison of mycobacterial Eis proteins.

The multiple sequence alignment was performed with ENDscript[40] and adjusted manually. The secondary structure (α, α-helix; β, β-strand, η, 3_{10}-helix) of $Eis1_{Mab}$ extracted from its crystal structure, is indicated above the alignment. Residues involved in ACO binding in $Eis1_{Mab}$ are indicated by the green circles, residues involved in aminoglycoside recognition in *M. tuberculosis* (Eis_{Mtb}) and *M. smegmatis* (Eis_{Msm}) Eis are depicted by the black and cyan square respectively.

Figure 6: Structural comparison of Eis proteins reveals unique features in $Eis1_{Mab}$.

A Superposition of Eis crystal structures. All the structures are displayed as a ribbon representation with the following color codes: $Eis1_{Mab}$ in slate, Eis_{Mtb} in yellow, $Eis2_{Mab}$ in raspberry, Eis_{Msm} in magenta, Eis_{Ban} in cyan, Eis_{Ava} in orange, Eis_{Efa} in salmon and Eis_{Kfl} in red. Superposition of the carbon α was performed in Coot. The arrow indicates the loop between strands 9 and 10 which appears particularly extended in $Eis1_{Mab}$. **B** Comparison of the volume (grey surface area) of the active sites of the structures of Eis proteins that have been biochemically characterized, the color code is the same as in A. For structures solved with either ACO or CoA, the cofactor is shown as yellow sticks. **C** Key structural features restricting the size of the $Eis1_{Mab}$ (slate) substrate-binding pocket. Arrows highlight the helices α4 and α5 movements seen in $Eis1_{Mab}$ as compare with Eis_{Mtb} (in yellow). $Eis1_{Mab}$ residues side chains that protrude towards the substrate binding-site are shown

as sticks and their equivalent residues in Eis_{Mtb} that are not pointing towards the substrate pocket are also indicated.

Figure 7: Comparison of the extended loop size and conformation

A Close up at the interface of two $Eis1_{Mab}$ monomers. The extended loop of monomer 2 in slate is covering the active site of monomer 1 (in white) and the Phe242 side chain is pointing towards the substrate-binding site of monomer 1 that is close to the ACO (stick representation) binding pocket. The superposition of Eis_{Mtb} structure (PDB id: 4JD6) bound to tobramycin in yellow, to $Eis1_{Mab}$ highlights the steric hindrance of Phe242, presumably preventing the binding of aminoglycosides. **B** Comparison of the same loop region with the one in other Eis crystal structures from various bacterial origins. Eis_{Mtb} is in yellow, Eis_{Msm} in magenta, Eis_{Ban} in cyan and, Eis_{Ava} in orange.

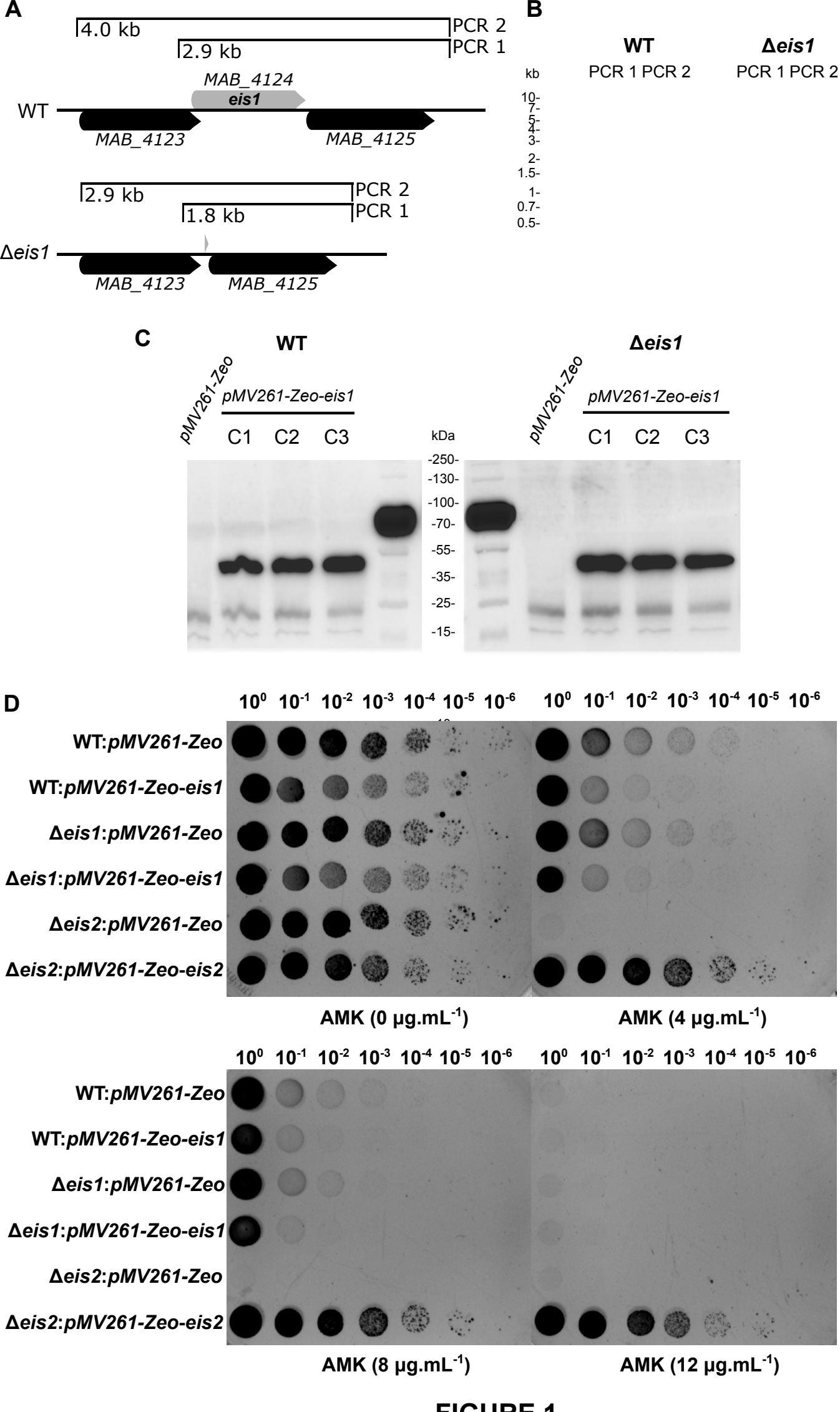
A
4.0 kb
PCR 2
2.9 kb
PCR 1
MAB_4124
eis1
WT
MAB_4123
MAB_4125
2.9 kb
PCR 2
1.8 kb
PCR 1
Δeis1
MAB_4123
MAB_4125
B
WT
Δeis1
kb
PCR 1 PCR 2
PCR 1 PCR 2
10-
7-
5-
4-
3-
2-
1.5-
1-
0.7-
0.5-
C
WT
Δeis1
pMV261-Zeo
pMV261-Zeo-eis1
C1 C2 C3
kDa
-250-
-130-
-100-
-70-
-55-
-35-
-25-
-15-
D
10^0 10^-1 10^-2 10^-3 10^-4 10^-5 10^-6
WT:pMV261-Zeo
WT:pMV261-Zeo-eis1
Δeis1:pMV261-Zeo
Δeis1:pMV261-Zeo-eis1
Δeis2:pMV261-Zeo
Δeis2:pMV261-Zeo-eis2
AMK (0 µg.mL-1)
AMK (4 µg.mL-1)
AMK (8 µg.mL-1)
AMK (12 µg.mL-1)

FIGURE 1

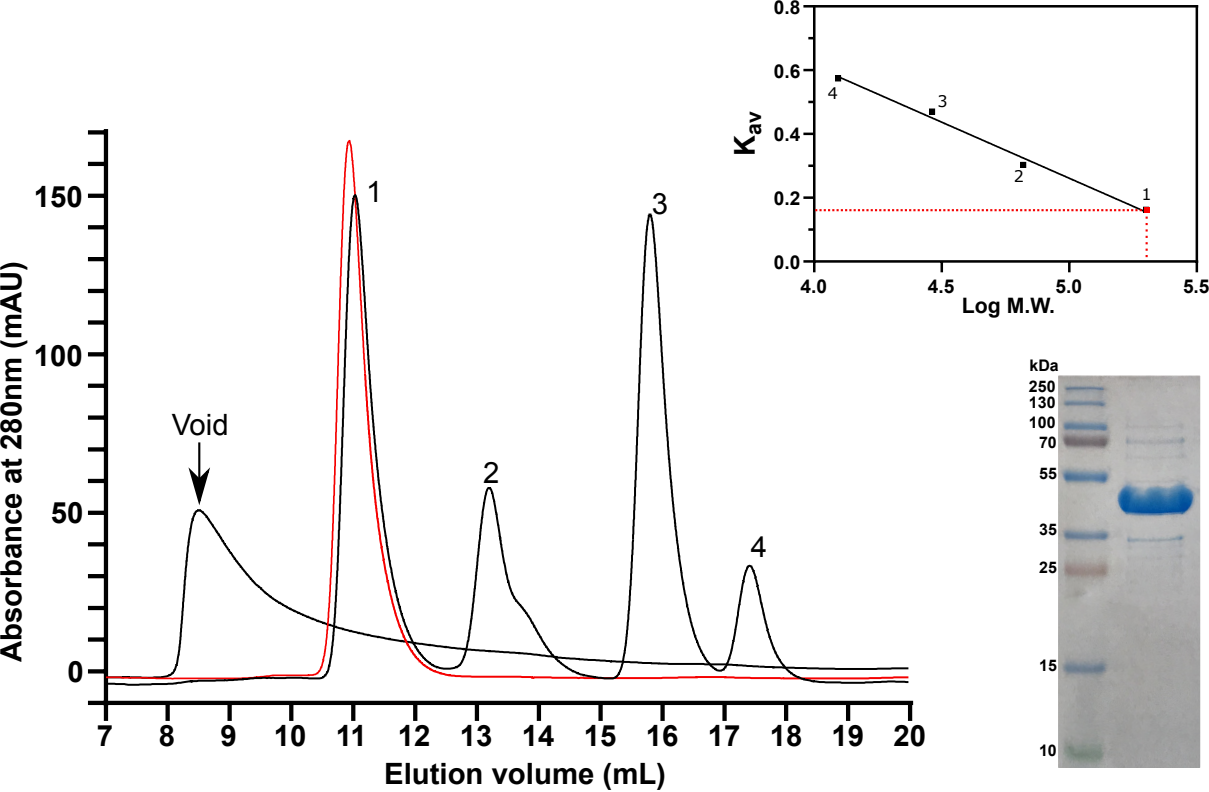
Absorbance at 280nm (mAU)
150
100
50
0
Void
1
2
3
4
7
8
9
10
11
12
13
14
15
16
17
18
19
20
Elution volume (mL)
K_{av}
0.8
0.6
0.4
0.2
0.0
4.0
4.5
5.0
5.5
Log M.W.
kDa
250
130
100
70
55
35
25
15
10

Figure 2

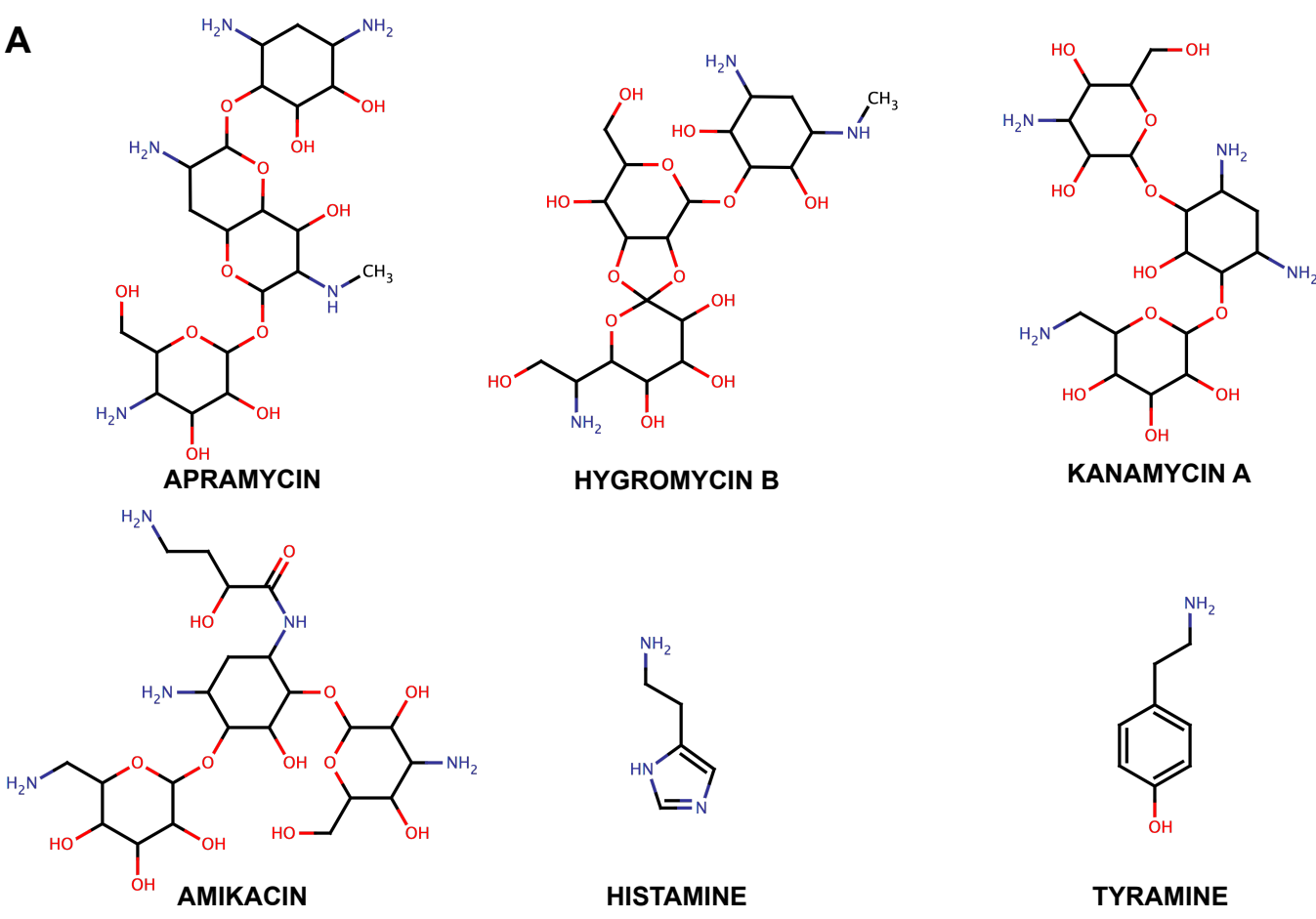
A
APRAMYCIN
HYGROMYCIN B
KANAMYCIN A
AMIKACIN
HISTAMINE
TYRAMINE

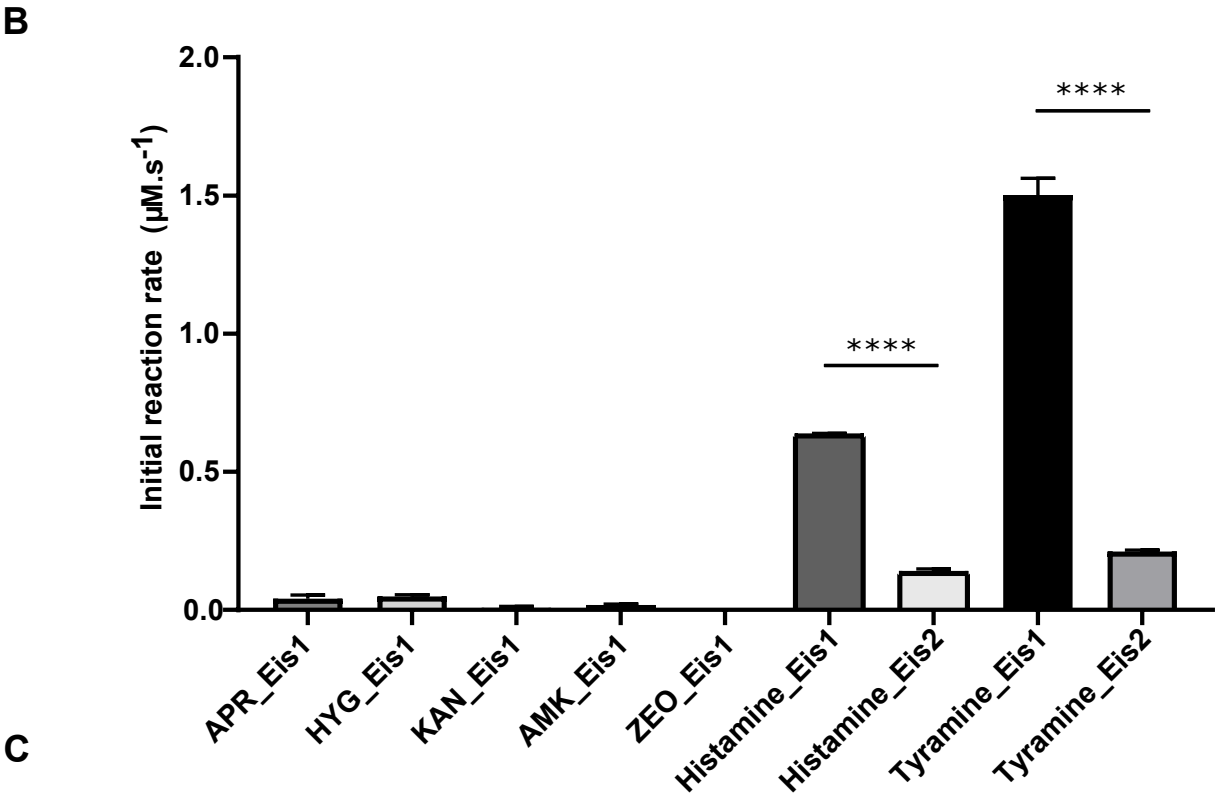
B
Initial reaction rate (µM.s-1)
2.0
1.5
1.0
0.5
0.0
****
****
APR_Eis1
HYG_Eis1
KAN_Eis1
AMK_Eis1
ZEO_Eis1
Histamine_Eis1
Histamine_Eis2
Tyramine_Eis1
Tyramine_Eis2

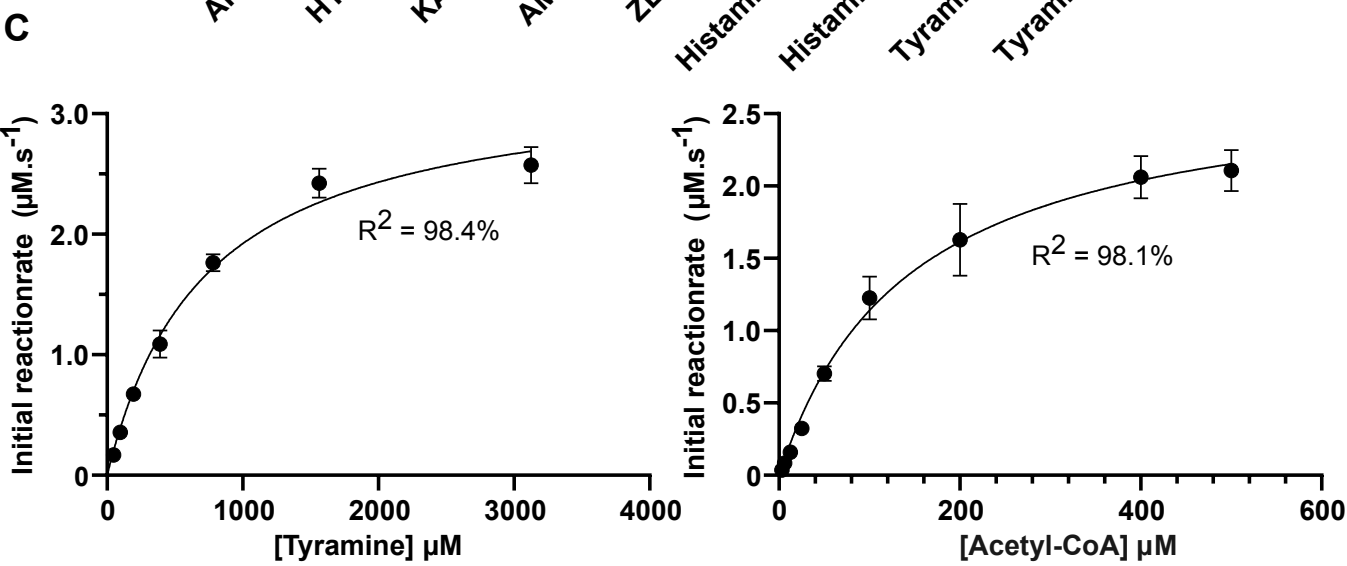
C
Initial reactionrate (µM.s-1)
3.0
2.0
1.0
0
R2 = 98.4%
0
1000
2000
3000
4000
[Tyramine] µM
Initial reactionrate (µM.s-1)
2.5
2.0
1.5
1.0
0.5
0
R2 = 98.1%
0
200
400
600
[Acetyl-CoA] µM

FIGURE 3

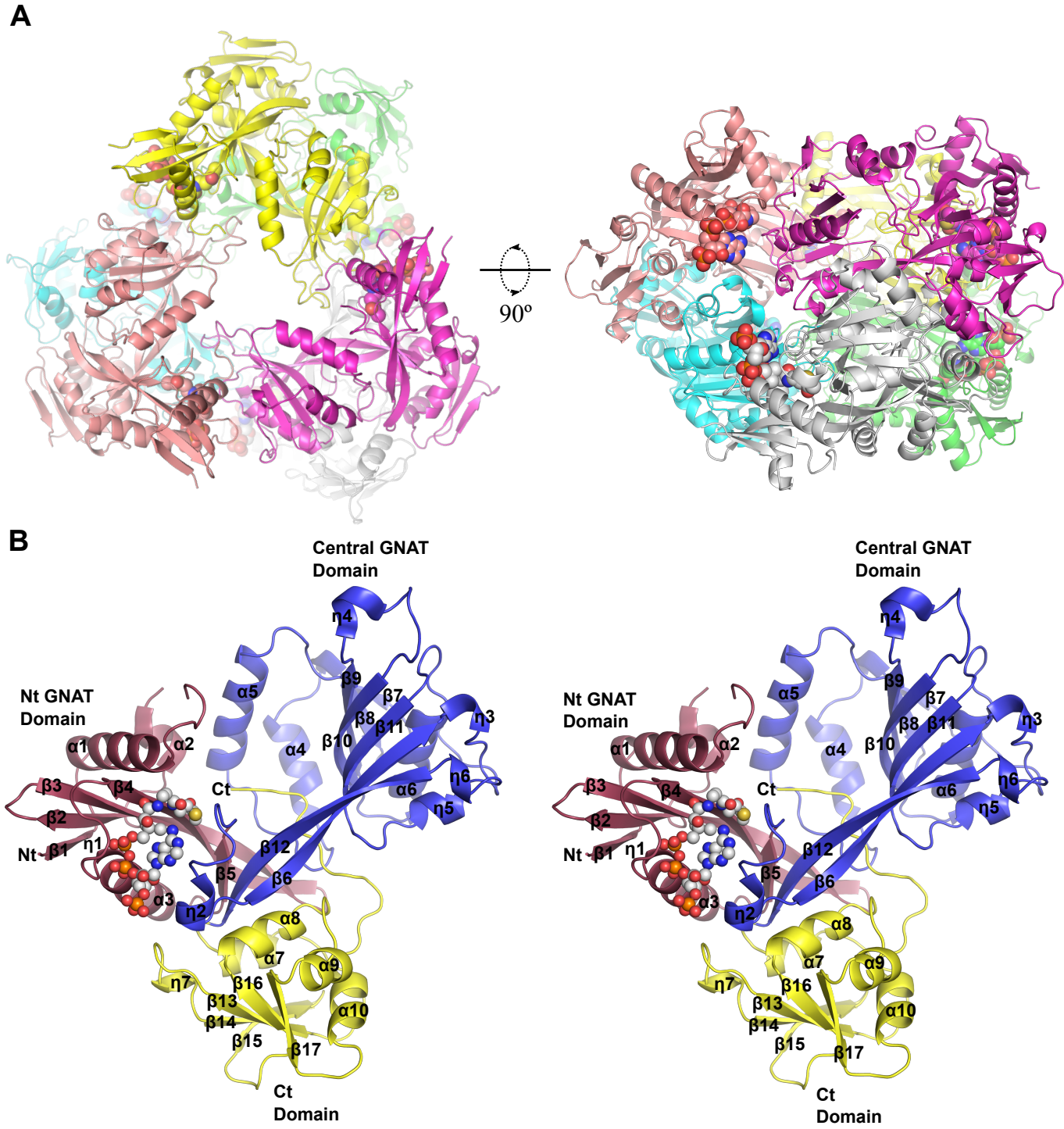
A
90°
B
Central GNAT Domain
Nt GNAT Domain
Ct Domain
Nt
Ct
η4
β9
β7
β8
β11
η3
α5
α4
β10
α1
α2
β3
β4
α6
η6
β2
η5
β1
η1
β12
β5
β6
α3
η2
α8
α7
α9
η7
β16
β13
β14
β15
β17
α10
C
D
V104
H101
R111
G112
I113
I102
R110
T115
L114
S138
L135
I142
E139
R145

FIGURE 4

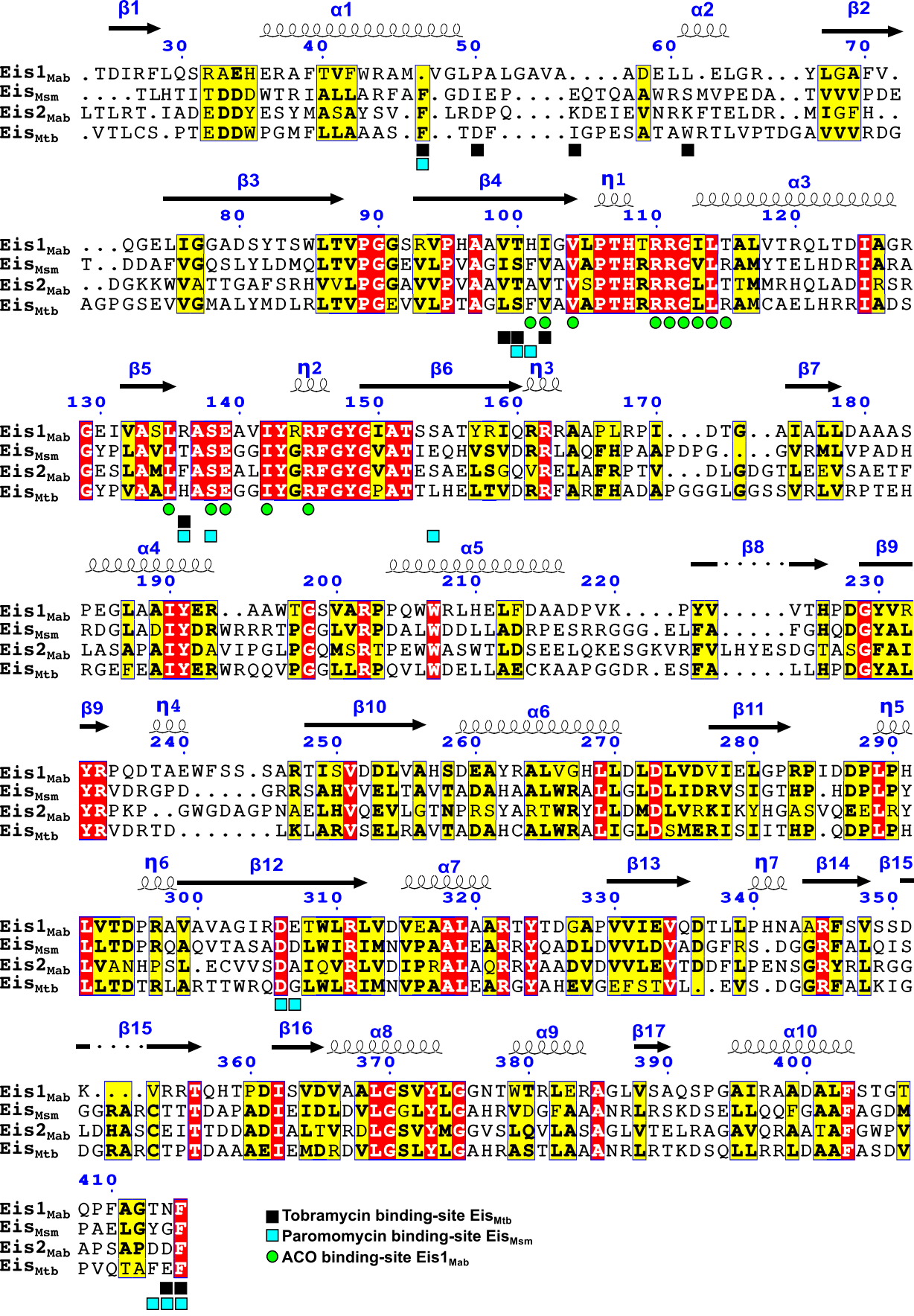
β1
α1
α2
β2
30
40
50
60
70
Eis1Mab .TDIRFLQSRAEHERAFTVFWRAM.VGLPALGAVA....ADELL.ELGR...YLGAFV.
EisMsm ....TLHTITDDDWTRIALLARFAF.GDIEP....EQTQAAWRSMVPEDA..TVVVPDE
Eis2Mab LTLRT.IADEDDYESYMASAYSV.F.LRDPQ....KDEIEVNRKFTELDR..MIGFH..
EisMtb .VTLCS.PTEDDWPGMFLLAAAS.F..TDF.....IGPESATAWRTLVPTDGAVVVRDG
β3
β4
η1
α3
80
90
100
110
120
Eis1Mab ...QGELIGGADSYTSWLTVPGGSRVPHAAVTHIGVLPTHTRRGILTALVTRQLTDIAGR
EisMsm T..DDAFVGQSLYLDMQLTVPGGEVLPVAGISFVAVAPTHRRRGVLRAMYTELHDRIARA
Eis2Mab ..DGKKWVATTGAFSRHVVLPGGAVVPVAAVTAVTVSPTHRRRGLLTTMMRHQLADIRSR
EisMtb AGPGSEVVGMALYMDLRLTVPGEVVLPTAGLSFVAVAPTHRRRGLLRAMCAELHRRIADS
β5
η2
β6
η3
β7
130
140
150
160
170
180
Eis1Mab GEIVASLRASEAVIYRRFGYGIATSSATYRIQRRRAAPLRPI...DTG..AIALLDAAAS
EisMsm GYPLAVLTASEGGIYGRFGYGVATIEQHVSVDRRLAQFHPAAPDPG...GVRMLVPADH
Eis2Mab GESLAMLFASEALIYGRFGYGVATESAELSGQVRELAFRPTV...DLGDGTLEEVSAETF
EisMtb GYPVAALHASEGGIYGRFGYGPATTLHELTVDRRFARFHADAPGGGLGGSSVRLVRPTEH
α4
α5
β8
β9
190
200
210
220
230
Eis1Mab PEGLAAIYER..AAWTGSVARPPQWWRLHELFDAADPVK....PYV.....VTHPDGYVR
EisMsm RDGLADIYDRWRRRTPGGLVRPDALWDDLLADRPESRRGGG.ELFA.....FGHQDGYAL
Eis2Mab LASAPAIYDAVIPGLPGQMSRTPEWWASWTLDSEELQKESGKVRFVLHYESDGTASGFAI
EisMtb RGEFEAIYERWRQQVPGGLLRPQVLWDELLAECKAAPGGDR.ESFA.....LLHPDGYAL
β9
η4
β10
α6
β11
η5
240
250
260
270
280
290
Eis1Mab YRPQDTAEWFSS.SARTISVDDLVAHSDEAYRALVGHLLDLDLVDVIELGPRPIDDPLPH
EisMsm YRVDRGPD.....GRRSAHVVELTAVTADAHAALWRALLGLDLIDRVSIGTHP.HDPLPY
Eis2Mab YRPKP..GWGDAGPNAELHVQEVLGTNPRSYARTWRYLLDMDLVRKIKYHGASVQEELRY
EisMtb YRVDRTD.......LKLARVSELRAVTADAHCALWRALIGLDSMERISIITHP.QDPLPH
η6
β12
α7
β13
η7
β14
β15
300
310
320
330
340
350
Eis1Mab LVTDPRAVAVAGIRDETWLRLVDVEAALAARTYTDGAPVVIEVQDTLLPHNAARFSVSSD
EisMsm LLTDPRQAQVTASADDLWIRIMNVPAALEARRYQADLDVVLDVADGFRS.DGGRFALQIS
Eis2Mab LVANHPSL.ECVVSDAIQVRLVDIPRALAQRRYAADVDVVLEVTDDFLPENSGRYRLRGG
EisMtb LLTDTRLARTTWRQDGLWLRIMNVPAALEARGYAHEVGEFSTVL..EVS.DGGRFALKIG
β15
β16
α8
α9
β17
α10
360
370
380
390
400
Eis1Mab K...VRRTQHTPDISVDVAALGSVYLGGNTWTRLERAGLVSAQSPGAIRAADALFSTGT
EisMsm GGRARCTTTDAPADIEIDLDVLGGLYLGAHRVDGFAAANRLRSKDSELLQQFGAAFAGDM
Eis2Mab LDHASCEITTDDADIALTVRDLGSVYMGGVSLQVLASAGLVTELRAGAVQRAATAFGWPV
EisMtb DGRARCTPTDAAAEIEMDRDVLGSLYLGAHRASTLAAANRLRTKDSQLLRRLDAAFASDV
410
Eis1Mab QPFAGTNF
EisMsm PAELGYGF
Eis2Mab APSAPDDF
EisMtb PVQTAFEF
Tobramycin binding-site EisMtb
Paromomycin binding-site EisMsm
ACO binding-site Eis1Mab

FIGURE 5

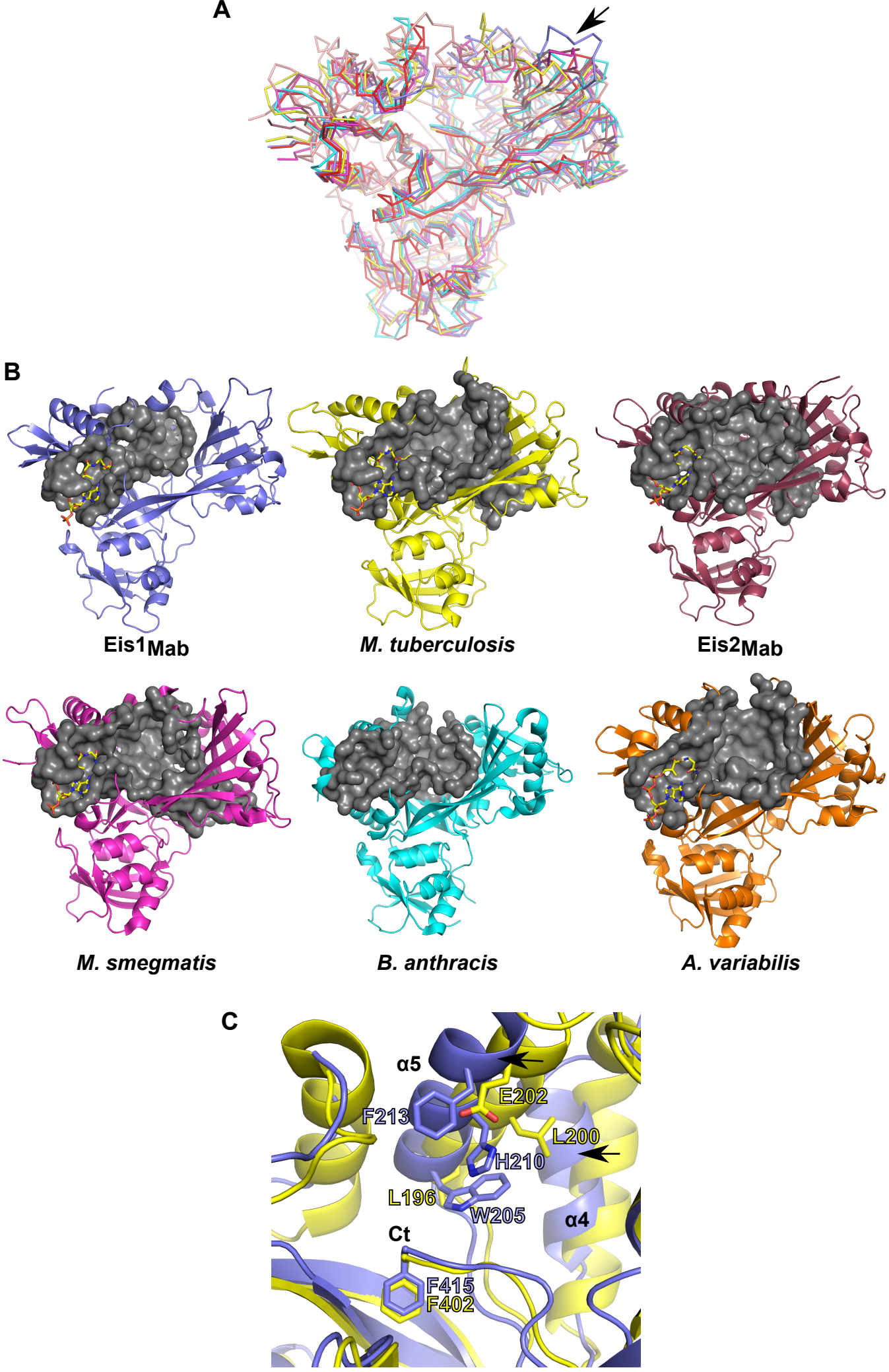
A
B
Eis1Mab
M. tuberculosis
Eis2Mab
M. smegmatis
B. anthracis
A. variabilis
C
α5
E202
F213
L200
H210
L196
W205
α4
Ct
F415
F402

FIGURE 6

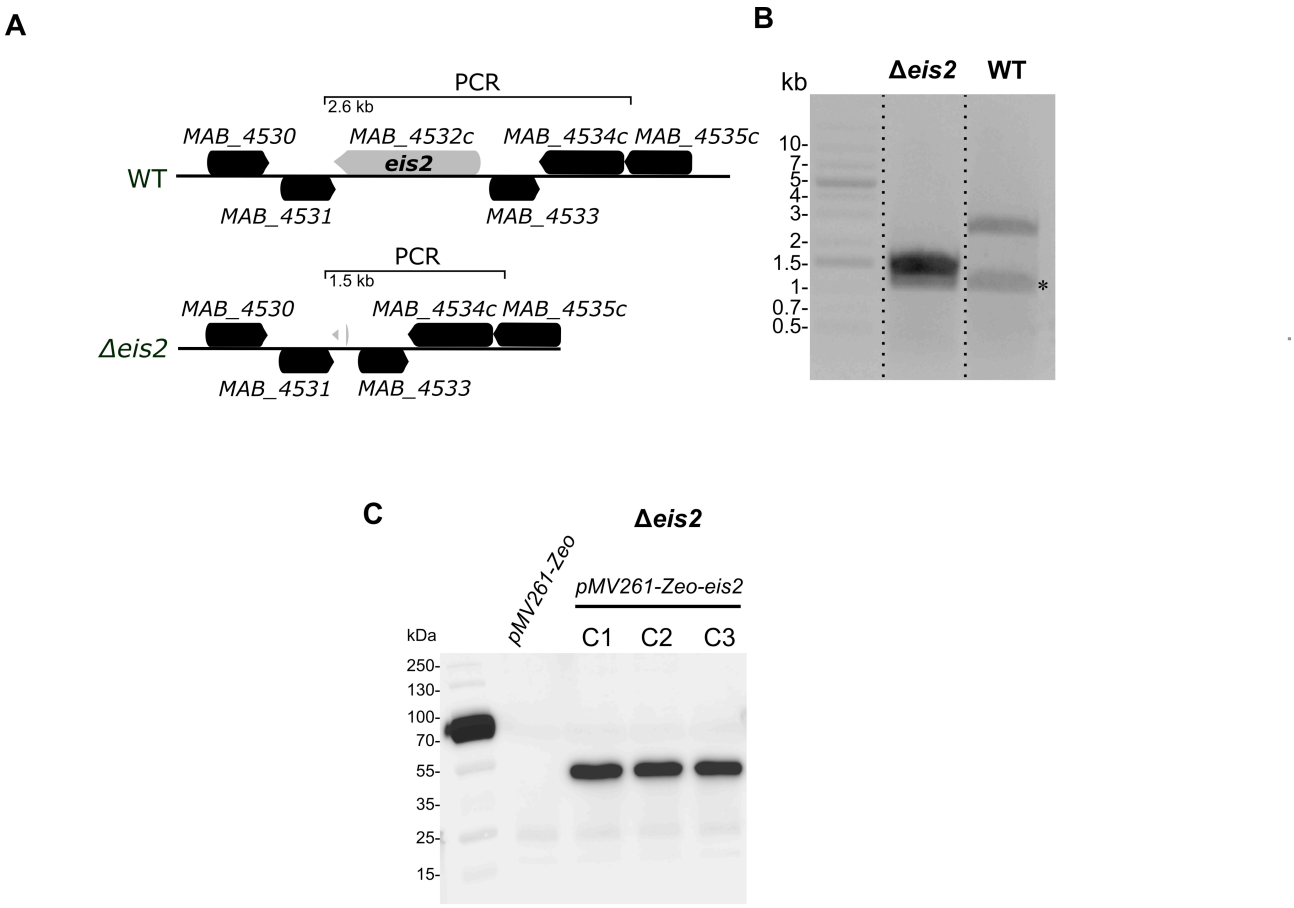

Supporting information Figure S1 : Generation of a Δ*eis2 M. abscessus* mutant and Eis2 overexpressing strain.

A Schematic representation of the genomic region around *eis2*$_{Mab}$ in the parental (WT) and Δ*eis2*$_{Mab}$ mutant strains of *M. abscessus*. Sizes of the PCR amplicons used for genotyping the Δ*eis2* mutant are shown. **B** PCR profile confirming the proper deletion of *eis2*$_{Mab}$ in the mutant strain. One PCR product of 1493 bp amplified from Δ*eis2*$_{Mab}$ mutant genomic DNA is expected while one band at 2657 bp is expected for the WT strain. * Indicates an unspecific amplicon at about 1 kb, systematically obtained with these set of primers using the mutant or WT genomic DNA templates. The dashed lines indicate that two lanes were cropped from the gel. **C** Protein expression pattern of Eis2$_{Mab}$ in the parental (WT) and knockout strains. Western blotting using anti-Strep-tag primary antibodies attest for the expression of Eis2$_{Mab}$ in the two strains transformed with pMV261-Zeo-*eis2* in three individual colonies (C1-C3). The strain transformed with the empty pMV261-Zeo was included as a negative control. The band at 70 kDa of the protein ladder possesses also a Strep-tag explaining its immune reactivity with the antibody.